

1 **Revision 2**

2 **Radiation effects in radioactive galena from burning heaps after coal mining from the**
3 **Lower Silesian basin (Czech Republic)**

4
5 MICHAL ČURDA^{1,2,*}, VIKTOR GOLIÁŠ¹, MARIANA KLEMENTOVÁ³, LADISLAV STRNAD⁴, ZDENĚK
6 MATĚJ⁵ AND RADEK ŠKODA⁶

7 ¹ Institute of Geochemistry, Mineralogy and Mineral Resources, Charles University, Faculty of Science,
8 Albertov 6, 128 43 Prague 2, Czech Republic; *email: michal.curda@geology.cz

9 ² Czech Geological Survey, Geologická 6, 152 00 Prague 5, Czech Republic

10 ³ Institute of Inorganic Chemistry, Czech Academy of Sciences, 250 68 Husinec-Řež, Czech Republic

11 ⁴ Laboratories of the Geological Institutes, Charles University, Faculty of Science, Albertov 6, 128 43 Prague 2,
12 Czech Republic

13 ⁵ Department of Condensed Matter Physics, Charles University, Faculty of Mathematics and Physics, Ke
14 Karlovu 5, 121 16 Prague 2, Czech Republic

15 ⁶ Institute of Earth Sciences, Faculty of Science, Masaryk University, Kotlářská 2, 611 37 Brno, Czech Republic
16

17 **ABSTRACT**

18 The isotopic composition of lead (²⁰⁷Pb/²⁰⁶Pb, ²⁰⁸Pb/²⁰⁶Pb and ²¹⁰Pb) in a recently-formed
19 galena from burning heaps after coal mining in Radvanice, Markoušovice and Rybníček, the
20 Lower Silesian basin, Czech Republic, was studied in detail. ²¹⁰Pb activity in galena varied
21 from 135 ± 9 Bq/g to 714 ± 22 Bq/g and calculated integral doses ranged from 2.21 × 10¹¹ α/g
22 to 6.11 × 10¹¹ α/g. The radioactivity of the galena causes micro-deformations in its crystal
23 structure as indicated by the Williamson-Hall graphs, showing that the level of micro-strain
24 depends on the length of time that galena samples were exposed to the radiation. However,
25 the crystal structure of galena is affected very inhomogeneously; according to TEM
26 investigations there are domains of fully crystalline, polycrystalline and fully metamict galena
27 within one crystal. Inductively coupled plasma mass spectrometry (ICP-MS) was used to
28 determine the isotopic composition of the studied galena. The stable isotope ratios of Pb
29 varied for ²⁰⁷Pb/²⁰⁶Pb from 0.8402 to 0.8435 and for ²⁰⁸Pb/²⁰⁶Pb from 2.0663 to 2.0836. The

30 average ratios $^{207}\text{Pb}/^{206}\text{Pb} = 0.8312$ and $^{208}\text{Pb}/^{206}\text{Pb} = 2.0421$ were obtained for coal from the
31 same localities. These isotope ratios show that there is no isotopic fractionation taking place
32 during the coal burning and subsequent galena crystallization from hot gases.

33

34 **Running title:** Radioactive galena from Czech Republic

35 **Keywords:** galena, radiation, lead-isotopes, radiation effects, metamict state

36

37

38

INTRODUCTION

39 ^{210}Pb is an isotope in the decay series of ^{238}U with a half-life of 22 years, where it is a long-
40 term radioactive daughter of ^{222}Rn . Thus, ^{210}Pb is usually enriched in metallic lead or galena
41 under conditions where there is long-term contact with radon (e.g., during natural gas
42 production) (Schmidt 1998; Schmidt et al. 2000).

43 Another geologic source of ^{210}Pb is outflow of hot volcanic gases through steam holes.
44 Increased levels of ^{210}Pb were described in sulphur crusts precipitated on the Vulcano Island
45 (Voltaggio et al. 1998) and on Mt. Etna (Le Cloarec et al. 1988; Le Cloarec and Pennisi
46 2001).

47 Groundwater in Triassic sandstone reservoirs with an elevated U content (up to 70
48 mg/kg) can be enriched in ^{210}Pb , as at the Wytch farm, southern UK. At Wytch farm water is
49 rich in sulphates and ^{226}Ra precipitates in barite, whereas ^{210}Pb remains in solution (Worden et
50 al. 2000).

51 Water enriched in ^{226}Ra occurs more commonly as chloride brines that originate from
52 sedimentary sequences rich in uranium. Such waters are known from the Polish side of the
53 described geological unit – the Lower Silesian Basin. Water pumped out from mines or from
54 boreholes exhibit rather high activity, up to 85.5 Bq/l ^{226}Ra (Kozłowska et al. 2010), which is

55 very high as compared to global values. Fresh groundwaters typically have on the order of
56 0.01 – 0.03 Bq/l ²²⁶Ra (Porcelli and Swarzenski 2003).

57 The Jestřebí Mountains with the Žaltman peak (739.1 m a.s.l.) are located in Eastern
58 Bohemia between the Krkonoše (Giant Mts.) and Orlické hory Mountains. Coal has been
59 mined in this area for more than 400 years in more than 200 mine workings (Jirásek 2006).
60 Besides coal, copper ore from copper-bearing shales enriched with sulphides (chalcocite and
61 bornite in nodules) and uranium from black coal beds bound onto Carboniferous sediments
62 were also mined there (Pešek et al. 2001). The resulting mine heaps contained a large amount
63 of lean coal enriched in Cu, U, Pb, Ge, Zn, Mo and other elements. The coal mass burnt on
64 some of the heaps through time and leaking gases produced newly-formed mineral phases by
65 desublimation. The richest (in terms of minerals and mineraloids) and also the most
66 investigated locality is Radvanice. Various newly formed minerals and mineraloids of Cd, In,
67 Ge, Zn, Bi, S etc. (e.g. greenockite, gunningite, GeO₂, Bi₂Te, GeS₂, GeAsS, GeSnS₃ etc.)
68 were described there (Sejkora et al. 1998b; Žáček and Ondruš 1997). Amongst these is
69 radioactive galena, the objective of the current study. As most localities have been remediated
70 and collecting samples is almost impossible, these samples are rare.

71

72 **GEOLOGICAL SETTINGS AND LOCALITY DESCRIPTION**

73 The Lower Silesian Basin, also referred to as the Žaclěř-Svatoňovice basin, is an upper-Paleozoic
74 limnic basin. Only one third of the entire area of the Lower Silesian Basin (about 1800 km²) lies in the Czech
75 Republic in the vicinity of Žaclěř and Broumov (Pešek et al. 2001; Hřebec and Veselý 1984; Sýkorová et al.
76 2016). Sedimentation in the basin started during the lower Carboniferous (Tournaisian) in the Polish portion, and
77 sedimentation subsequently expanded to the Bohemian portion (Visean). At the beginning of the Visean, a sea
78 flooded the entire area. However; at the end of this period the sea retreated and purely continental sedimentation
79 (with some hiatuses) proceeded from the Carboniferous to the middle Triassic. Coal beds were formed during the
80 Carboniferous in a humid climate (Pešek et al. 2001; Chlupáč et al. 2011; Košťák et al. 2011).

81

82 *Radvanice – the Kateřina I mine (50°33'39.963"N, 16°3'58.648"E)*

83 The main inclined shaft of the Kateřina I mine was opened in 1901 and served originally for black coal
84 mining. Uranium mining operated by the Jáchymovské doly state enterprise mining company was performed
85 there from 1953 until 1957, when a portion of the deposit was transferred the Východočeské uhelné doly (VUD,
86 Eastern Bohemian coal mines) company. The mine was closed in 1993 (Cimala 1997; Jirásek 2003). An
87 estimated 500,000 t of black coal and 60,000 t of radioactive coal were mined between 1952 and 1957. With an
88 average grade of 0.29 % U in the coal it, mining recovered a total of 387.2 t of U (Sejkora et al. 1998a; Kafka
89 2003; Pauliš et al. 2007). Total black coal production from 1901 to 1994 is estimated at 10,500,000 t of coal
90 (Cimala 1997).

91 The Kateřina I mine heap had an aerial extent of 40,000 m² (approximately 200 x 200 m) and a height
92 reaching to 60 m. About 2,300,000 m³ of mine waste was deposited there, 20% of which was radioactive lean
93 coal remaining after uranium ore mining (Sejkora et al. 1998a). The exact time of heap-flaring is unknown.
94 Initial attempts to extinguish the fire occurred from 1967 to 1969. Preparations for the final quenching started in
95 November 1979. The remediation was finished at the end of 2006 (Němec 2006).

96 All galena samples from Radvanice were collected in 1998, when the heap was still burning, and the
97 desublimation processes were active. Galena crystallised in deeper portions of the heap, at least 0.5 m beneath
98 the surface. The temperature in the zone of crystallisation was 600–800 °C. Under such high temperatures the
99 reductive association of metallic Pb, Sb, Bi (as liquid droplets), and Sb-Bi, Sn-Bi, Sn-Ge and Pb-Sn
100 intermetallics were associated with galena (Sejkora and Tvrđý 1999). Galena formed as free, highly-lustrous
101 (some tarnished) crystals, growing on the burnt rock. Crystals ranged from several millimeters up to 1.5 cm in
102 diameter (Fig. 1), with masses from 0.024 g to 0.384 g, with an average of 0.122 g.

103

104 *Markoušovice locality – the Ignác mine (50°33'33.170"N, 16°0'35.890"E)*

105 Coal mining in the surroundings of Markoušovice has a long and colorful history. Coal was mined there
106 for more than 400 years, and is one of the oldest and longest operated mining districts in Bohemia. Mining
107 operations ended in 1899 due to exploitation and flooding. Although uranium mineralisation lenses appear in the
108 mined Bukov beds, the locality was classified uneconomical in the 1950s and uranium was not recovered
109 (Jirásek 2003; Jirásek 2006).

110 The heap near the village of Markoušovice measures about 150–200 m in to dimensions, and has a
111 height of about 20 m. 36,000 m³ of waste material was deposited in these heaps. The coal mass fraction is

112 estimated at 40 %, i.e., approx. 18,000 t of coal. The heap flared in 2006. The fire was ignited by forest workers
113 burning waste wood. The fire was extinguished and remediation was complete in 2007 (Jirásek et al. 2008;
114 Pauliš and Kopecký 2010).

115 Galena samples selected for study from Markoušovice are tiny hexahedral crystals forming crust
116 covering a 10 cm diameter rock fragment (Fig. 2). Tarnishing was common.

117

118 *Rybníček locality – the Novátor mine (50°37'49.436"N, 15°58'51.838"E)*

119 The Novátor mining operation was located in the Bečkov and Rybníček cadastral areas, and had mine
120 several workings in the early Permian Rybníček radioactive bed. Prospecting for uranium was performed from
121 1947 to 1953. After uranium mining between 1952 and 1957, the mines were transferred to the Východočeské
122 uhelné doly (VUD) mining company for recovery of the remaining black coal from the columns. However, the
123 mine closed three years later. A total of 170.8 t U was mined here (Cimala 1997; Kafka 2003; Pauliš et al. 2007).

124 There are 13 coal heaps around the villages of Rybníček and Bečkov. Five of these contain an elevated
125 fraction of radioactive coal. The shaft No. 3 heap is formed by several ridges of approximately height 25 m.
126 100,000 m³ of material were deposited on an area of about 12,000 m² (Kříbek et al. 2008). The heap flared about
127 1960. Today it is covered with birch, beech and spruce trees. The mineralogy of this locality was described by
128 Sejkora et al. (1998b). The Rybníček locality provided only tiny efflorescences of galena and one small, strongly
129 corroded crystal covered by anglesite (Fig. 3).

130

131

EXPERIMENTAL METHODS

132 *Gamma-spectrometry*

133 The activity of ²¹⁰Pb in the samples studied here was measured using a laboratory low-background
134 anticompton-anticoincidence gamma spectrometer SILAR (Faculty of Science, Charles University, Prague),
135 which is designed for measurements of low activities of low-energy γ -emitters in small volumes (Hamrová et al.
136 2010). The ²¹⁰Pb 47 keV energy was selected for mass activity determination, because strong sample matrix
137 effects of PbS are expected even at such a low γ energy. Shielding due to the heavy matrix was accounted for by
138 measuring 20 individual galena crystals, where the lower mass activity was detected in the cases of larger grains
139 (radiation from the crystal core is absorbed effectively by the layers close to the surface). We therefore chose a
140 constant mass measurement process, where the matrix effect is constant for all samples. A 50 mg portion of
141 milled galena in 1 mL AXYGEN ST 050 plastic bottle was measured for 1 hour. No standards or reference

142 material are available for this material (^{210}Pb in galena), so a secondary standard with a similar matrix and ^{210}Pb
143 activity that approximates the studied samples was prepared. A 0.0020 g portion of radiogenic lead primary
144 standard (SRM 983, NIST, USA) was ground to a powder, and had a certified ^{210}Pb activity of 16 kBq/g (in
145 December 2004, the reference year). The activity was calculated for the current date, and the standard powder
146 was diluted with 0.048 g of non-radioactive galena from the Příbram – Březové Hory deposit, which had a U
147 activity lower than the detection limit (< 0.06 mg/kg). This artificial galena secondary standard had a ^{210}Pb
148 activity of 484 Bq/g (on 24th May 2014).

149

150 *Alpha-spectrometry*

151 Non-destructive semi-conductor alpha-spectrometry was used to determine and evaluate the presence of
152 alpha-active radionuclides in the samples. A powder sample was prepared from galena from the Radvanice site.
153 A suspension of the galena powder was placed on a holder and dried. The sample weight was 280 μg , as
154 determined by a micro-balance. The spectrum was collected over 24 hours using a semi-conductor alpha detector
155 PIPS 450 mm² (CANBERRA). The signal was processed by the multi-channel analyser CANBERRA Series 10.

156

157 *Alpha-autoradiography*

158 The distribution of radionuclides in the galena matrix was investigated using the alpha autoradiography
159 method. A film LR – 115A (KODAK) was placed on top of a polished section from the Radvanice sample, and
160 the film was exposed for one week. Subsequently the film was developed using standard etching methods in a 10
161 % NaOH solution at 60 °C.

162

163 *Powder X-ray diffraction*

164 Powder X-ray diffraction (PXRD) was performed utilizing an X'Pert Pro (PANalytical) diffractometer
165 operating with $\text{CuK}\alpha$ radiation. Data collection was done for the range of 24–80° 2θ with a step 0.02° 2θ and a
166 counting time of 300 s/step (continuous mode). The HighScore Plus (PANalytical) with PDF – 2 (ICDD, 2003)
167 database was used for phase analysis. Profile fitting was done using HighScore Plus (PANalytical) and the
168 pseudo-Voigt profile function, which was chosen because it provided the best fits to the experimental profiles.
169 This function is a sum of Gauss and Cauchy functions with a free parameter weighing both components (Kužel
170 2003). Unit cell parameters of galena were refined using the least squares method by the HighScore Plus
171 (PANalytical) program. The diffraction data were corrected for shift of the sample from the goniometer plane

172 (sample displacement).

173 The LaB₆ standard was used for testing the resolution of the instrument (*FWHM*). A synthetic PbS
174 sample was prepared in the Laboratory of Experimental Mineralogy of the Czech Geological Survey to compare
175 the structure of natural and synthetic material.

176

177 *Transmission electron microscopy*

178 Transmission electron microscopy (TEM) was carried out on a JEOL JEM 3010 microscope operated at
179 300 kV (LaB₆ cathode, point resolution 1.7Å) with an Oxford Instruments Energy Dispersive X-ray (EDX)
180 detector attached. Images were recorded on a CCD camera with resolution 1024x1024 pixels using the Digital
181 Micrograph software package. Electron diffraction patterns were evaluated using the Process Diffraction
182 software package (Lábár 2005). Powder samples were dispersed in ethanol and the suspension was treated by
183 ultrasound for 5 minutes. A drop of very dilute suspension was placed on a holey-carbon-coated copper grid and
184 allowed to dry by evaporation at ambient temperature.

185

186 *Electron-probe microanalysis*

187 Qualitative and quantitative chemical analyses were performed using a CAMECA SX-100 electron
188 microprobe equipped with four crystal spectrometers (operator M. Fridrichová, Institute of Geology, ASCR,
189 v.v.i.). A TESCAN Vega scanning electron microscope with an EDS X-max 50 (Oxford Instruments) detector
190 and acceleration voltage 15 kV, beam current 1.5 nA was used for BSE imaging (operator M. Racek, Faculty of
191 Science, Charles University, Prague).

192

193 *Mass spectrometry*

194 Uranium, lead and thorium contents, as well as the isotopic ratios of Pb were measured using a X Series
195 II Thermo Scientific quadrupole mass spectrometer (operator L. Strnad, Faculty of Science, Charles University,
196 Prague). Galena samples were dissolved in 10 mL of concentrated HNO₃. After evaporation, a further 5 mL of
197 concentrated HNO₃ was added and the solution was evaporated again. The remaining salts were placed in 25
198 mL HDPE bottles filled with 2 % (v/v) HNO₃. Coal samples were ground and 0.5 g ± 0.0005 g of material was
199 placed on platinum plates and fired in a furnace at 450 °C for four hours. The maximum temperature was
200 reached after gradual increasing the temperature at a rate of 50 °C/60 min. HClO₄ and HF were used for
201 mineralisation of the ashes. For details of the analytical protocol and correction strategy see Strnad et al. (2005)

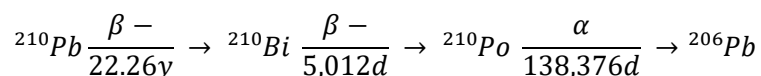
202 and Ďurišová et al. (2015). The external reproducibility of this method was monitored using the reference
203 material NIST 1632b (Bituminous coal, NIST, USA). ^{74}Ge , ^{103}Rh and ^{187}Re isotopes were used as internal
204 standards. Standard reference material SRM 981 (Common lead, NIST, USA) and SRM 983 (Radiogenic lead,
205 NIST, USA) were used for lead isotope measurement verification.

206

207

RESULTS

208 When the coal heap material enriched in uranium caught fire, Pb – including its
209 radioactive isotope ^{210}Pb – was released into the escaping gases. The liberated Pb was
210 incorporated within the structure of galena during crystallization due to de-sublimation of
211 hot gases. The radioactivity of this recently-formed galena is caused by the presence of
212 radioactive ^{210}Pb and its decay products that have accumulated in the galena structure. The
213 studied galena contains radionuclides of the ^{238}U decay chain, specifically at least its three
214 final radionuclides as well as the final daughter, stable (non-radioactive) Pb, respectively:



215 A major part of the γ activity of the studied galena is caused by secondary nuclear effects
216 associated with the high β activity ^{210}Bi with very “hard” energy ($\beta_{\text{max}} = 1.162$ MeV). For the
217 heavy galena matrix, the characteristic radiation lines Pb-X (72.8 to 84.9 keV, lines PbK β and
218 PbK α composite) appears and Bremsstrahlung is also strongly emitted up to the energy
219 corresponding to the above mentioned β_{max} . These effects are apparent in the γ spectrum of
220 the galena from Radvanice (Fig. 4).

221 Alpha-spectrometry revealed the main α emitter is ^{210}Po ($E_{\alpha} 5304$ keV), which is a
222 daughter after ^{210}Pb (Fig. 5). ^{212}Po ($E_{\alpha} = 8785$ keV) from the ^{232}Th decay chain was also
223 detected in almost negligible amounts. As there are no lead isotopes having a longer lifetime
224 in that decay chain, mechanical contamination from the surrounding rock is the most probable
225 explanation (Fig. 5).

226 According to the autoradiographic picture, different α track densities (corresponding
227 with ^{210}Po α activity) are present in different crystals (Fig. 6). This is perhaps due to an
228 uneven burning of the inhomogenous heap material (with respect to the U and thus also ^{210}Pb
229 content). The PbCl_2 vapors were the most likely transport medium for lead (Wang and Tomia
230 2003). Ammonium chloride crusts found in the overburden of the crystallised galena from
231 Radvanice strongly support this theory.

232 At the time the samples were collected from the burning Radvanice heap, the galena
233 radioactivity was very high and decreased rapidly within a few hours (indicated by qualitative
234 Geiger counter measurements by R. Škoda). This may have been caused by the presence of
235 the short-lived radionuclides ^{214}Pb ($t^{1/2} = 26.8$ min) and ^{214}Bi ($t^{1/2} = 19.9$ min), which were
236 also originally present in newly-formed galena.

237 Due to the short half-life of ^{210}Pb ($t^{1/2} = 22.26$ years), the total activity of this nuclide
238 in galena has decreased significantly since crystallization. Today, the average radioactivity of
239 galena from Radvanice is 624 ± 59 Bq/g (the galena age is 16 years). Galena from
240 Markoušovice has a measured activity of 684 ± 20 Bq/g (the galena age is 8 years), and for
241 Rybníček galena the activity is only 135 ± 9 Bq/g (the galena age is about 50 years). As the
242 ages of the galena crystals are known the original mass activity of ^{210}Pb at the time of
243 crystallisation can be calculated. The original activity of Radvanice galena is 1026 Bq/g
244 (integral dose for the 16 years is 4.34×10^{11} α/g), that of Markoušovice galena is 877 Bq/g
245 (dose for the 8 years is 2.21×10^{11} α/g), and that of Rybníček galena is 724 Bq/g (dose for the
246 ~ 54 years is 6.11×10^{11} α/g). The activity of the galena samples at the time of their formation
247 is quite similar at all studied localities (Fig. 7). The calculated integral dose of the galena
248 samples studied is quite low. For example, the integral dose is seven orders of magnitude
249 lower than in some cases of metamict zircon, where the typical dose is up to $12\text{-}14 \times 10^{18}$ α/g
250 (e.g. Farnan et al. 2007, Nasdala et al. 2005, and others).

251 Broadening of powder diffraction profiles in the studied galena samples shows a
252 strong anisotropy, *i.e.* a strong hkl -dependence. This is typical due to contributions from
253 defects such as dislocations or stacking faults. Such an anisotropy was observed previously in
254 studies of Ungár et al. (1999) in ball-milled galena. For studies of structural micro-
255 deformation in such materials it is more convenient to use a modified form of the Williamson-
256 Hall plot method. XRD line broadening due to lattice defects is sensitive, similar to electron
257 microscopy, to the mutual orientation of hkl diffraction vectors and dislocation lines, as well
258 as to the character of the deformation fields, and can be strongly influenced by the crystal
259 elastic anisotropy. For the powder diffraction case this can be accounted for by “dislocation
260 orientation factors” C_{hkl} (Ungár et al. 1999). The expected linear dependence of XRD line
261 broadening on the length of the diffraction vector ($\sin \theta$) is then modified by the square root
262 of the orientation factors C_{hkl} . In case of the cubic material the orientation factors C_{hkl} are a
263 simple function of the well-known cubic Γ_{hkl} invariant:

$$C_{hkl} = C_{h00} * (1 + q\Gamma_{hkl}), \quad \text{where} \quad q\Gamma_{hkl} = \frac{h^2k^2 + k^2l^2 + l^2h^2}{(h^2 + k^2 + l^2)^2} \quad (1)$$

264 Parameters C_{h00} and q above are material constants characteristic of the dislocation
265 type (edge or screw) and the active dislocation slip system. These can be calculated using
266 theory provided in Klimánek and Kužel (1988) or *e.g.*, the software ANIZC (ANIZC, 2003).
267 It was shown that for many materials the C_{h00} constant is very similar for edge and screw
268 dislocations of a particular slip system, whereas parameter q differs significantly. The most
269 common slip system for *fcc* materials is $\{111\}\langle 110 \rangle$; however, for galena the $\{100\}\langle 110 \rangle$ slip
270 system was reported to be most active (Deeb et al. 2004). Ungár et al. (2002) reported a high
271 $q = 6.5$ value calculated for the Zener anisotropy ratio of PbS $A_z = 0.311$. A calculation based
272 on the general theory (Klimánek and Kužel 1988) and using Wolfram Mathematica gives $q_s =$
273 1 for $\langle 110 \rangle$ screw dislocations and $q_e = 4.3$ for $\{100\}\langle 110 \rangle$ edge dislocations. Hence the q
274 parameter was optimized to obtain the best linear correlation in the modified Williamson-Hall

275 plot assuming that it is in the range of 1.0 to 4.3. In our case a higher q equates to stronger
276 hkl -anisotropy. The density of dislocation defects is then proportional to the slope in the
277 modified Williamson-Hall plot (Fig. 8). Samples from Radvanice, Příbram and synthetic PbS
278 show strong anisotropy, hence $q = 4.3$ was used and the modified Williamson-Hall plot gives
279 better a correlation than the simple linear version, whereas for samples from localities in
280 Markoušovice and Rybníček the anisotropy is not so strong, and the modified method does
281 not provide significant improvement and consequently a lower q ($= 1$) was used. Concerning
282 the crystallite size and micro-deformation, the graph shows (Fig. 8) that the size-effect on
283 diffraction line broadening is unimportant, but the presence of strain in galena caused by
284 micro-deformations varies within samples. The lowest values of micro-strain are observed for
285 synthetic galena, which should ideally contain no micro-deformations, although this is not the
286 case. Rapid cooling of synthetic galena upon removal from the furnace may have caused this
287 difference from the ideal state. The structure data of the studied galena show that the extent of
288 crystal structure damage depends on the duration of the radiation exposure. A high level of
289 strain occurs for Rybníček galena (age ~ 50 years), and lower values occur for Radvanice
290 galena (age is 16 years). The galena sample from Markoušovice (age is 8 years) exhibits the
291 lowest structural damage. These micro-deformations are caused by the presence of the ^{210}Pb
292 emitter and its daughters that produce destructive ionizing particles (mainly α and recoil
293 daughters) in the crystal structure of galena.

294 Investigations using HRTEM showed that micro-deformations in galena from
295 Radvanice are caused mainly by metamictization of the galena structure. Three stages of
296 structure damage were observed: 1) fully crystalline, 2) polycrystalline (nano-crystalline) and
297 3) fully metamict (“amorphous” PbS) (Fig. 9). We find it very interesting that fully metamict
298 galena occurs as a ball-like crystalline cluster of nanometric size (Fig 9 / 4b). This feature
299 probably represents a process of self-recrystallization of amorphous PbS, as was also

300 documented for metamict zircon (e.g. Palenik et al. 2003, Ewing et al. 2003) and in other
301 minerals containing radioactive elements (Ewing et al. 2000).

302 The existence of distinct degrees of structural damage within one sample (macro-
303 crystal) could relate to the primary differences in initial ^{210}Pb content in galena, caused by
304 various ^{210}Pb activities in the gases that gradually were produced in burning heap material. A
305 significant zoning of the galena crystals is apparent in the autoradiographic images,
306 supporting this explanation. Another possible contributing factor is migration of structure
307 defects and their concentration into insulated clusters with the highest damage (Yashuda et al.
308 2003; Katoh et al. 2012). This situation is completely different from those observed in
309 materials such as zircon or other metamict minerals studied to date, which are all dielectrics.
310 Galena is a natural semiconductor (Jenkins 2005), so electrons, holes and also lattice defects
311 can migrate very readily.

312 The chemical compositions of galena samples from Radvanice, Markoušovice and
313 Rybníček are relatively homogeneous and there is only a small concentration of minor
314 elements that has no significant effect on the unit cell parameters of the studied galena.
315 Empirical formulae are: for Markoušovice galena
316 $(\text{Pb}_{0.96}\text{Sn}_{0.02}\text{Cd}_{0.01})_{\Sigma 0.99}(\text{S}_{0.97}\text{Se}_{0.03})_{\Sigma 1.00}$, Rybníček galena $(\text{Pb}_{0.97}\text{Cd}_{0.02}\text{Sn}_{0.01})_{\Sigma 1.00}(\text{S}_{0.94}\text{Se}_{0.07})_{\Sigma 1.01}$
317 and Radvanice galena $(\text{Pb}_{1.00}\text{Sn}_{0.01})_{\Sigma 1.01}(\text{S}_{0.95}\text{Se}_{0.03})_{\Sigma 0.98}$. Refined unit cell parameter a varies
318 between 5.934(4) Å and 5.9426(5) Å (with corresponding $V = 208.97(9)$ and $209.86(5)$ Å³).
319 These are in good agreement with results given by Vávra and Losos (1992), Žáček and
320 Ondruš (1997), and Sejkora et al. (1998a), who studied galena from the Radvanice locality.

321 Average isotopic ratios of lead from the heap material from the localities Radvanice,
322 Markoušovice and Rybníček are in the range ($^{207}\text{Pb}/^{206}\text{Pb}$) from 0.8213 to 0.8466 and
323 ($^{208}\text{Pb}/^{206}\text{Pb}$) from 2.0176 to 2.0791. These values correspond well with data of Mihaljevič et
324 al. (2009), where the most general value for Czech coal lies in the range ($^{207}\text{Pb}/^{206}\text{Pb}$) from

325 0.8333 to 0.8403, as well as for the value representing the upper crust with the isotopic ratio
326 ($^{207}\text{Pb}/^{206}\text{Pb}$) = 0.8333 (Novák et al. 2003). Similar values were measured in galena formed by
327 direct crystallization from gas produced by heap burning at the localities Markoušovice
328 ($^{207}\text{Pb}/^{206}\text{Pb}$) = 0.8402, Radvanice ($^{207}\text{Pb}/^{206}\text{Pb}$) = 0.8411, and Rybníček ($^{207}\text{Pb}/^{206}\text{Pb}$) =
329 0.8435. The isotopic ratios in coal, burnt rock and galena are considered equal and no
330 fractionation of lead occurs during heap burning, when lead is released from the coal mass
331 into the gases and consequently crystallizes in the form of galena.

332

333

IMPLICATIONS

334 Radiation damage in sulphides has been observed and described for the first time for
335 the case of recently-formed galena from burning heaps of U-rich coal. The high radioactivity
336 of the galena samples is caused by the presence of ^{210}Pb , its decay products (^{210}Bi and ^{210}Po),
337 as well as by secondary radiation, caused by nuclear effects of the interaction of the ^{210}Bi
338 isotope hard β rays with a heavy PbS matrix. ^{210}Pb in galena originates from the uranium-rich
339 coal. This lead isotope incorporates, together with non-radioactive isotopes, during heap
340 burning. Our investigations confirmed that the ^{210}Pb isotope and products of its decay-chain
341 cause strain and metamictization of the galena structure, as shown by PXRD and HRTEM.
342 This leads to formation of micro-deformations, represented by increased strain in the
343 structure, and by local structure degradation leading to an “amorphous” galena. Although
344 galena activities at the time of their formation were similar for all localities studied, their
345 structures are affected differently. Observed micro-strain is thus dependent mainly on the age
346 of the galena, *i.e.* on how long their crystal structures were exposed to radiation. Due to a
347 short half-life of ^{210}Pb (22.3 years), the activity of samples stored in mineral collections
348 decreases rapidly; for our followers they will no-longer be detectable, but the radiation
349 damage of their structures will be recorded.

350

351

ACKNOWLEDGEMENTS

352 This study was financially supported by the Czech Science Foundation grant (GACR 15-11674S) „A model of
353 mobilization and geochemical cycles of potentially hazardous elements and organic compounds in burned coal
354 heaps“. We would like to thank Václav Jirásek and Petr Rus for providing us galena samples and Marie
355 Fayadová for help with laboratory work on sample preparation.

356

357

REFERENCES CITED

- 358 Borbély, A., Dragomir-Cernatescu, J., Ribárik, G., and Ungár, T. (2003) Computer program
359 ANIZ for the calculation of diffraction contrast factors of dislocations in elastically
360 anisotropic cubic, hexagonal and trigonal crystals. *Journal of Applied Crystallography*,
361 36, 160–162.
- 362 Cimala, Z. (1997) Tracking prospecting and mining of uranium deposits in Moravia and
363 Eastern Bohemia, 130 p. O.z. GEAM Dolní Rožínka and SOO OS PHGN, Dolní
364 Rožínka (in Czech).
- 365 Deeb, C., Castaing, J., Walter, P., Penhoud, P., Veyssiére, P., and Martinetto, P. (2004)
366 Dislocations in Milled Galena (PbS). *Metallurgical and Materials Transactions A*, 35,
367 2223–2228.
- 368 Ďurišová, J., Ackerman, L., Strnad, L., Chrastný, V., and Borovička, J. (2015) Lead Isotopic
369 Composition in Biogenic Certified Reference Materials Determined by Different ICP-
370 based Mass Spectrometric Techniques. *Geostandards and Geoanalytical Research*, 39,
371 209–220.
- 372 Ewing, R.C., Alkiviathes, M., Wang, L., and Wang, S. (2000) Radiation-Induced
373 Amorphization. *Reviews in Mineralogy and Geochemistry*, 39, 317–361.
- 374 Ewing, R.C., Meldrum, A., Wang, L., Weber, W.J., and Corrales, L.R. (2003) Radiation
375 effects in zircon. *Reviews in Mineralogy and Geochemistry*, 53, 387–425. Farnan, I.,
376 Cho, H., and Weber, W.J. (2007) Quantification of actinide α -radiation damage in
377 minerals and ceramics. *Nature*, 445 (7124), 190–193.
- 378 Hamrová, E., Goliáš, V., and Petroušek, A. (2010) Identifying century – old long – spined
379 Daphnia: species replacement in a mountain lake characterised paleogenetic methods.
380 *Hydrobiologia*, 643, 97–106.
- 381 Hřebec, J., and Veselý, T. (1984) Small uranium deposits in Permian-carboniferous rocks in
382 Bohemian Massif. *Geologie a hydrometalurgie uranu*, 8, 27–54. (in Czech)
- 383 Chlupáč, I., Brzobohatý, R., Kovanda, J., and Stráník, Z. (2011) Geological history of the
384 Czech Republic, 436 p. Academia, Praha. (in Czech)
- 385 Jenkins, T. (2005) A brief history of semiconductors. *Physics education*, 40, 430.
- 386 Jirásek, V. (2003) Under the hammer and a pick symbol 1., 206 p. Nakladatelství Bor,
387 Liberec. (in Czech)
- 388 Jirásek, V. (2006) Black coal mining in the Markoušovice-Svatoňovice area in Jestřebí

- 389 Mountains, 87 p. Tiskárna PRATR, Trutnov. (in Czech)
- 390 Jirásek, V., Pauliš, P., and Kořátko, L. (2008) Minerals of the Ignác colliery burning heap in
391 Markoušovice near Trutnov. *Minerál*, 3, 233–237. (in Czech)
- 392 Kafka J., Ed. (2003) Ore and uranium mining in the Czech Republic, 647 p. Nakladatelství
393 ANAGRAM. (in Czech)
- 394 Katoh, Y., Snead, L.L., Szlufarska, I., and Weber, W.J. (2012) Radiation effects in SiC for
395 nuclear structural applications. *Current Opinion in Solid State and Materials Science*,
396 13, 143–152.
- 397 Klimánek, P., and Kužel, R. (1988) X-ray diffraction line broadening due to dislocations in
398 non-cubic materials. I. General considerations and the case of elastic isotropy applied to
399 hexagonal crystals. *Journal of Applied Crystallography*, 21, 59–66.
- 400 Košťák, M., Mazuch, M., Opluštil, S., Kraft, P., Marek, J., Fatka, O., Kachlík, V., Sakala, J.,
401 Martínek, K., Holcová, K., Kvaček, Z., and Žák, J. (2011) Travelling through our
402 prehistory, 192 p. Granit, s.r.o., Praha. (in Czech)
- 403 Kozłowska, B., Walencik, A., Przylibski, T.A., Dorda, J., and Zipper, W. (2010) Uranium,
404 radium and radon isotopes in selected brines of Poland. *Nukleonika*, 55, 519–522.
- 405 Kříbek, B., Malec, J., Barnett, I., Knésl, I., and Lukeš, P. (2008) Biogeochemical accumulation
406 of heavy metals on the abandoned coal and uranium mine heap in Bečkov near Žaclěb,
407 167-172 p. Zprávy o geologických výzkumech v roce 2007, Czech Geological Survey.
408 (in Czech)
- 409 Kužel, R. (2003) Information about powder diffractogram and its processing. *Materials*
410 *Structure*, 10, 32–33. (in Czech)
- 411 Lábár, J.L. (2005) Consistent indexing of a (set of) SAED pattern(s) with the
412 ProcessDiffraction program. *Ultramicroscopy*, 103, 237–249.
- 413 Le Cloarec, M.F., Lambert, G., and Ardouin, B. (1988) Isotopic enrichment of 210-Pb in
414 gaseous emissions from Mount Etna (Sicily). *Chemical Geology*, 70, 128.
- 415 Le Cloarec, M.F., and Pennisi, M. (2001) Radionuclides and sulfur content in Mount Etna
416 plume in 1983-1995: new constraints on the magma feeding system. *Journal of*
417 *Volcanology and Geothermal Research*, 108, 141–155.
- 418 McClune, W.F., International Centre for Diffraction Data (ICDD) (2003), Powder Diffraction
419 File. Diffraction Data, Newtown Square, Pennsylvania.
- 420 Mihaljevič, M., Ettler, V., Strnad, L., Šebek, O., Vonásek, F., Drahotka, P., and Rohovec, J.
421 (2009) Isotopic composition of lead in Czech coals. *International Journal of Coal*
422 *Geology*, 78, 38–46.
- 423 Nasdala, L., Hanchar, J.M., Kronz, A., and Whitehouse, M.J. (2005) Long-term stability of
424 alpha particle damage in natural zircon. *Chemical Geology*, 220(1), 83–103.
- 425 Němec, I. (2006) Removal of a burning heap. Remediation and restoration of the Kateřina
426 colliery heap. *Vesmír*, 85, 624–625. (in Czech)
- 427 Novák, M., Emmanuel, S., Vile, M.A., Erel, Y., Véron, A., Pačes, T., Wieder, R.K., Vaněček,
428 M., Štěpánová, M., Břízová, E., and Hovorka, J. (2003) Origin of Lead in Eight Central
429 European Peat Bogs Determined from Isotope Ratios, Strengths, and Operation Times
430 of Regional Pollution Sources. *Environmental Science & Technology*, 37, 437–445.
- 431 Palenik, C.S., Nasdala, L., and Ewing, R.C. (2003) Radiation damage in zircon. *American*

- 432 Mineralogist, 88(5-6), 770–781.
- 433 Pauliš, P., Kopecký, S., and Černý, P. (2007) Uranium minerals of the Czech Republic and
434 their localities. 2nd part, 252 p. Kuttna, Kutná Hora. (in Czech)
- 435 Pauliš, P., and Kopecký, S. (2010) The most interesting mineralogical localities in Bohemia,
436 Moravia and Silesia III, 112 p. Kuttna, Kutná Hora. (in Czech)
- 437 Pešek, J., Holub, V., Jaroš, J., Malý, L., Martínek, K., Prouza, V., Spudil, J., and Tásler, R.
438 (2001) Geology and deposits of the upper-palaeozoic limnic basins in the Czech
439 Republic, 243 p. Český geologický ústav, Praha. (in Czech)
- 440 Porcelli, D., and Swarzenski, P.W. (2003) The Behavior of U- and Th-series Nuclides in
441 Groundwater. Reviews in Mineralogy and Geochemistry, 52, 317–361.
- 442 Sejkora, J., Šrein, V., and Litochleb, J. (1998a) Lead minerals (native lead, galena, anglesite)
443 from burning heaps of the Kateřina colliery in Radvanice near Trutnov. Bulletin
444 mineralogicko-petrologického oddělení Národního muzea (Praha), 6, 232–237. (in
445 Czech)
- 446 Sejkora, J., Litochleb, J., Tvrđý, J., and Šrein, V. (1998b) Mineral association of the Kateřina
447 colliery burning heap in Radvanice near Trutnov and processes of its formation, 164–
448 166 p. Zprávy o geologických výzkumech v roce 1997, Czech Geological Survey,
449 Praha. (in Czech)
- 450 Sejkora, J., and Tvrđý J. (1999) Minerals of the Kateřina colliery burning heap in Radvanice
451 near Trutnov. Minerál, 5, 399–409. (in Czech)
- 452 Schmidt, A.P. (1998) Lead precipitates from natural gas production installations. Journal of
453 Geochemical Exploration, 62, 193–200.
- 454 Schmidt, A.P., Hartog, F.A., Os, van B.J.H., and Schuiling, R.D. (2000) Production of Pb-210
455 from a Schlochten Sandstone gas reservoir. Applied Geochemistry, 15, 1317–1329.
- 456 Strnad, L., Mihaljevič, M., and Šebek, O. (2005) Laser ablation and solution ICP-MS
457 determination of REE in USGS BIR-1G, BHVO-2G and BCR-2G glass reference
458 materials. Geostandards and Geoanalytical Research, 29, 303–314.
- 459 Sýkorová, I., Kříbek, B., Havelcová, M., Machovič, V., Špaldoňová, A., Lapčák, L., Kněsl, I.,
460 and Blažek, J. (2016) Radiation- and self-ignition induced alterations of Permian
461 uraniferous coal from the abandoned Novátor mine waste dump (Czech Republic).
462 International Journal of Coal Geology, 168, 162–178.
- 463 Vávra, V., and Losos, Z. (1992) New findings about secondary minerals from a burning heap
464 in Radvanice near Trutnov. Geologický Průzkum, 4, 101–102. (in Czech)
- 465 Ungár, T., Dragomir, I., Révész, Á., and Jenkins, A. (1999) The contrast factors of
466 dislocations in cubic crystals: the dislocation model of strain anisotropy in practice.
467 Journal of Applied Crystallography, 32, 9920–1002.
- 468 Ungár, T., Martinetto, P., Ribárik, G., Dooryhée, E., Walter, Ph., and Anne, M. (2002)
469 Revealing the powdering methods of black makeup in Ancient Egypt by fitting
470 microstructure based Fourier coefficients to the whole x-ray diffraction profiles of
471 galena. Journal of Applied Physics, 91, 2455.
- 472 Voltaggio, M., Tuccimei, P., Brance, M., and Romoli, L. (1998) U-series disequilibrium
473 radionuclides in sulphur incrustations from fumarolic field of Vulcano Island.
474 Geochimica et Cosmochimica Acta, 52, 2111–2127.

- 475 Wang, J., and Tomita, A. (2003) A Chemistry on the Volatility of Some Trace Elements
476 during Coal Combustion and Pyrolysis. *Energy & Fuels*, 17, 954–960.
- 477 Worden, R.H., Manning, D.A.C., and Lythgoe, P.R. (2000) The origin and production
478 geochemistry of radioactive lead (Pb-210) in NORM-contaminated formation waters.
479 *Journal of Geochemical Exploration*, 69, 695–699.
- 480 Yashuda, K., Kinishita, C., Matsumura, S., and Ryazanov, A.I. (2003) Radiation-induced
481 defects clusters in fully stabilized zirconia irradiated with ions and/or electrons. *Journal*
482 *of Nuclear Materials*, 319, 74–80.
- 483 Žáček, V., and Ondruš, P. (1997) Mineralogy of recently formed sublimates from the Kateřina
484 colliery in Radvanice, Eastern Bohemia, Czech Republic. *Věstník Českého*
485 *geologického ústavu*, 72, 289–302. (in Czech)
- 486

487 Figure captions

488 **Figure 1.** Free galena skeletal crystals. Radvanice (Photo: P. Škácha 2014).

489 **Figure 2.** A burnt rock with galena. Markoušovice (Photo: P. Škácha 2014).

490 **Figure 3.** A burnt rock with galena covered with anglesite. Rybníček (Photo: P. Škácha
491 2014).

492 **Figure 4.** Presence of ^{210}Pb in the γ -spectrum of galena from Radvanice.

493 **Figure 5.** An α -spectrum of galena: ^{210}Po is the main emitter, ^{212}Po is also detected as in
494 negligible amount.

495 **Figure 6.** Autoradiography of galena. a) polished section scan, b) SEM/EDS images, c) α
496 particle tracks on autoradiography.

497 **Figure 7.** A comparison of activity of ^{210}Pb in galena samples from Radvanice, Markoušovice
498 and Rybníček at the time of measurements (year 2014) and at the time of formation
499 (crystallisation).

500 **Figure 8.** Modified Williamson-Hall plot showing the micro-strain in crystal structure of
501 studied galena based on PXR data.

502 **Figure 9.** HRTEM images showing structural damage caused by radiation emitted by ^{210}Pb in
503 galena crystals. Different stages of metamictization are observed within one crystal. 1a), 1b),
504 1c) – well crystalline galena from Příbram (reference sample of fully crystalline galena); 2a),
505 2b), 2c) – crystalline stage in galena from Radvanice; 3a), 3b), 3c) – polycrystalline stage in
506 galena from Radvanice; 4a), 4b), 4c) – metamict stage in galena from Radvanice.

Figure 1

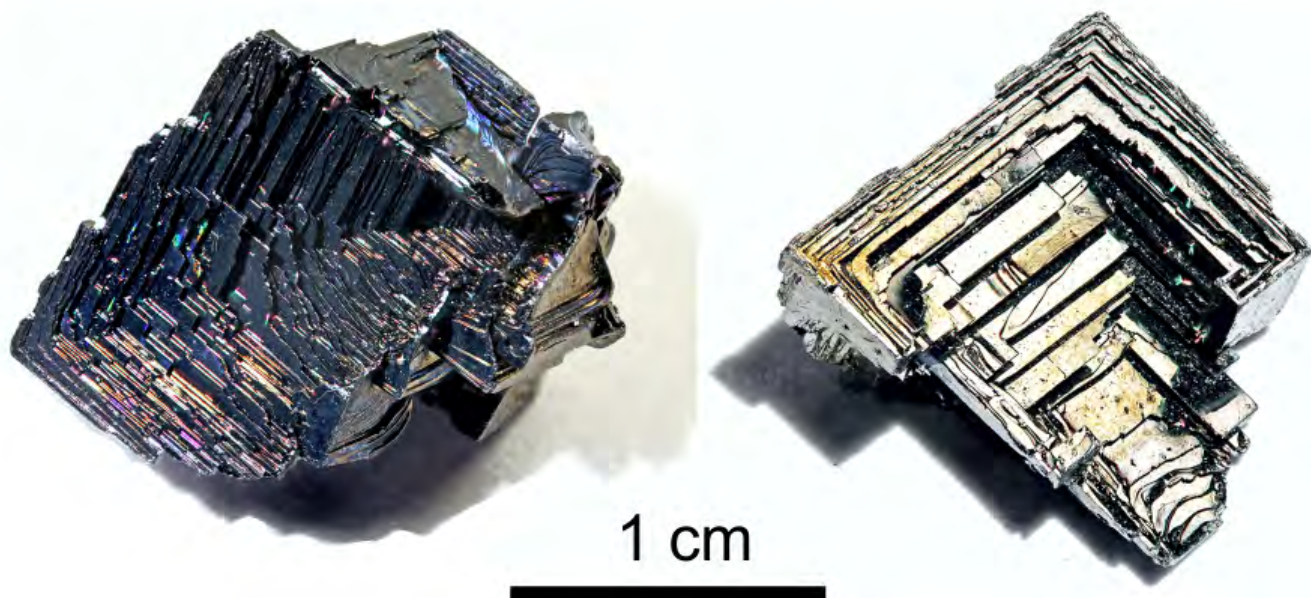


Figure 2



Figure 3

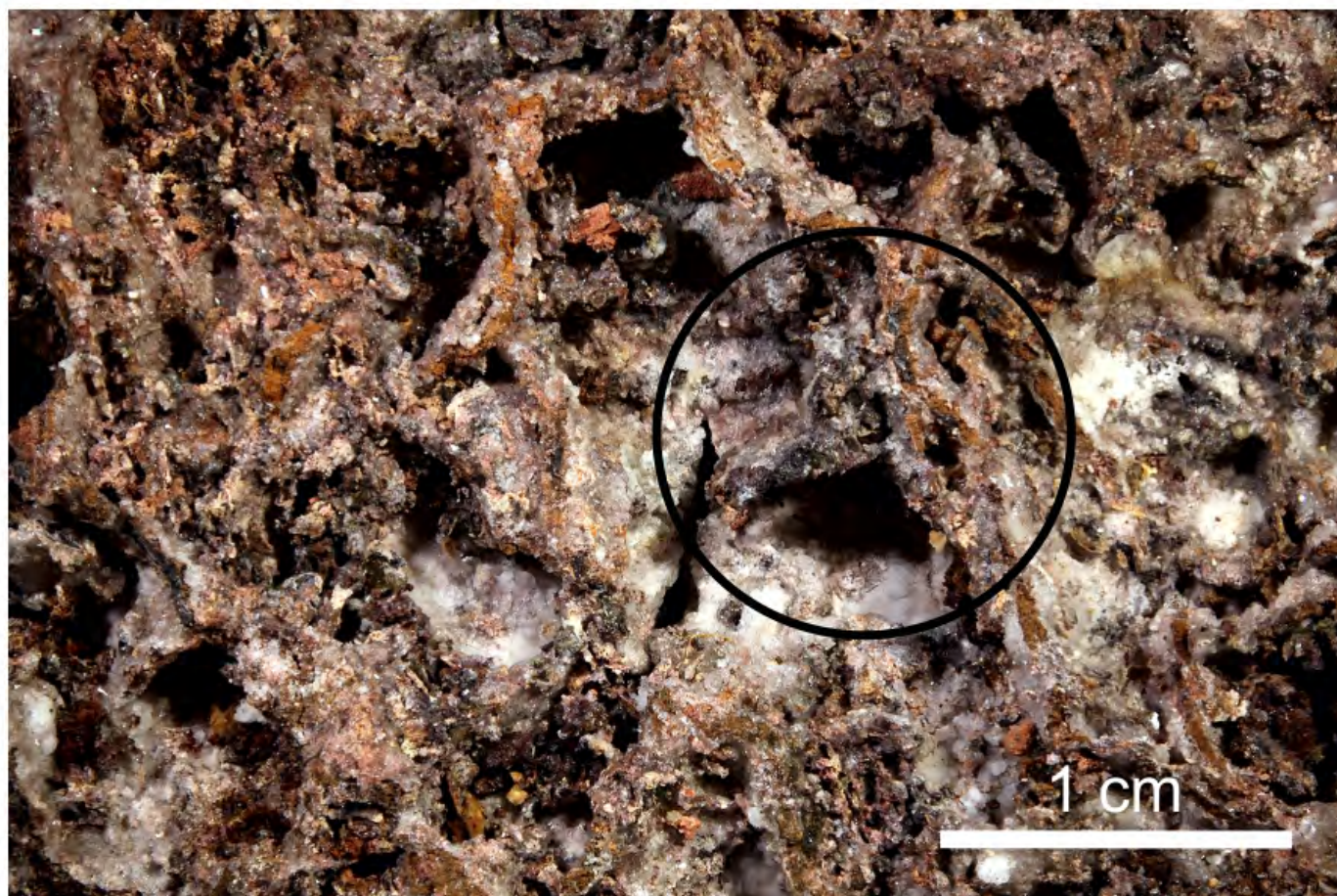


Figure 4

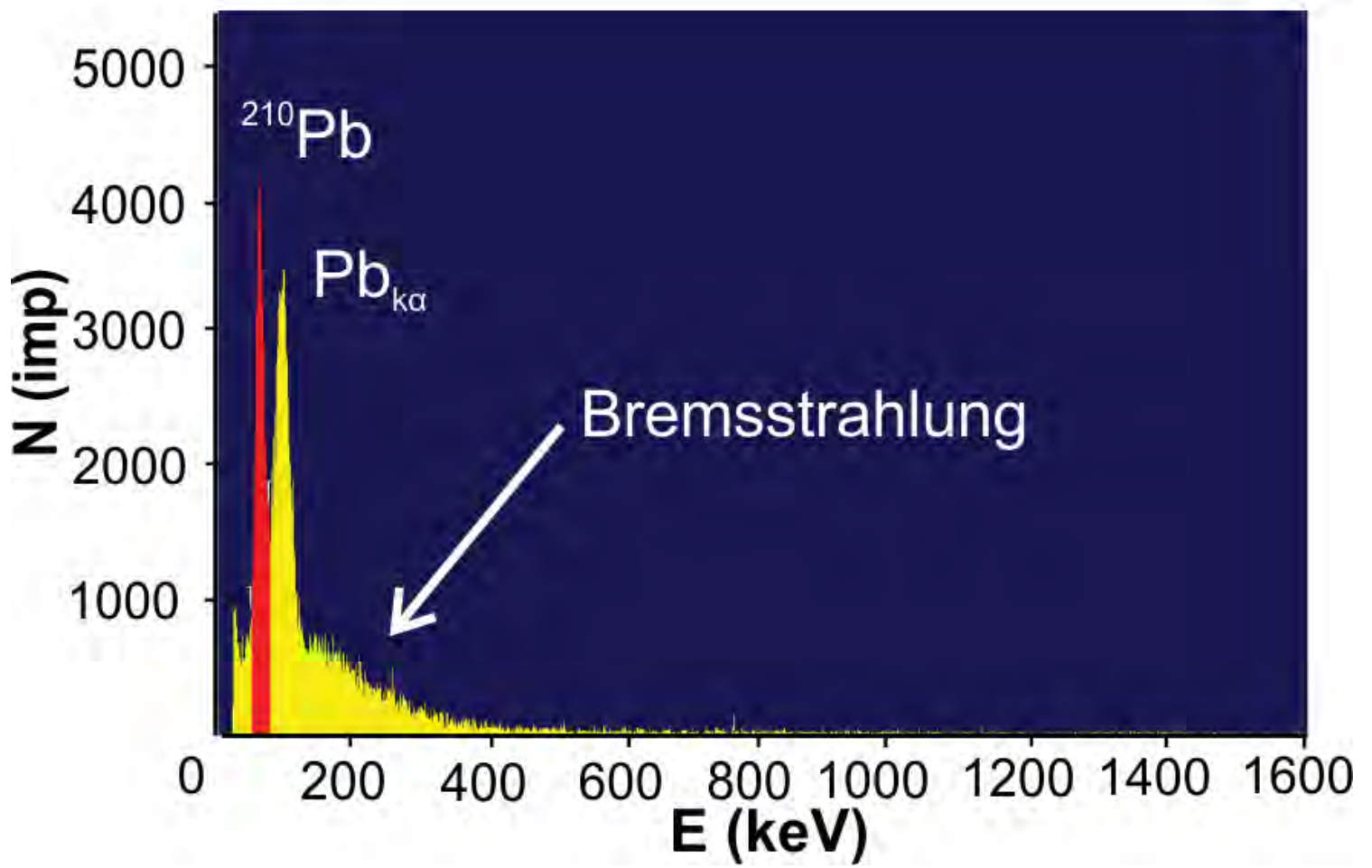


Figure 5

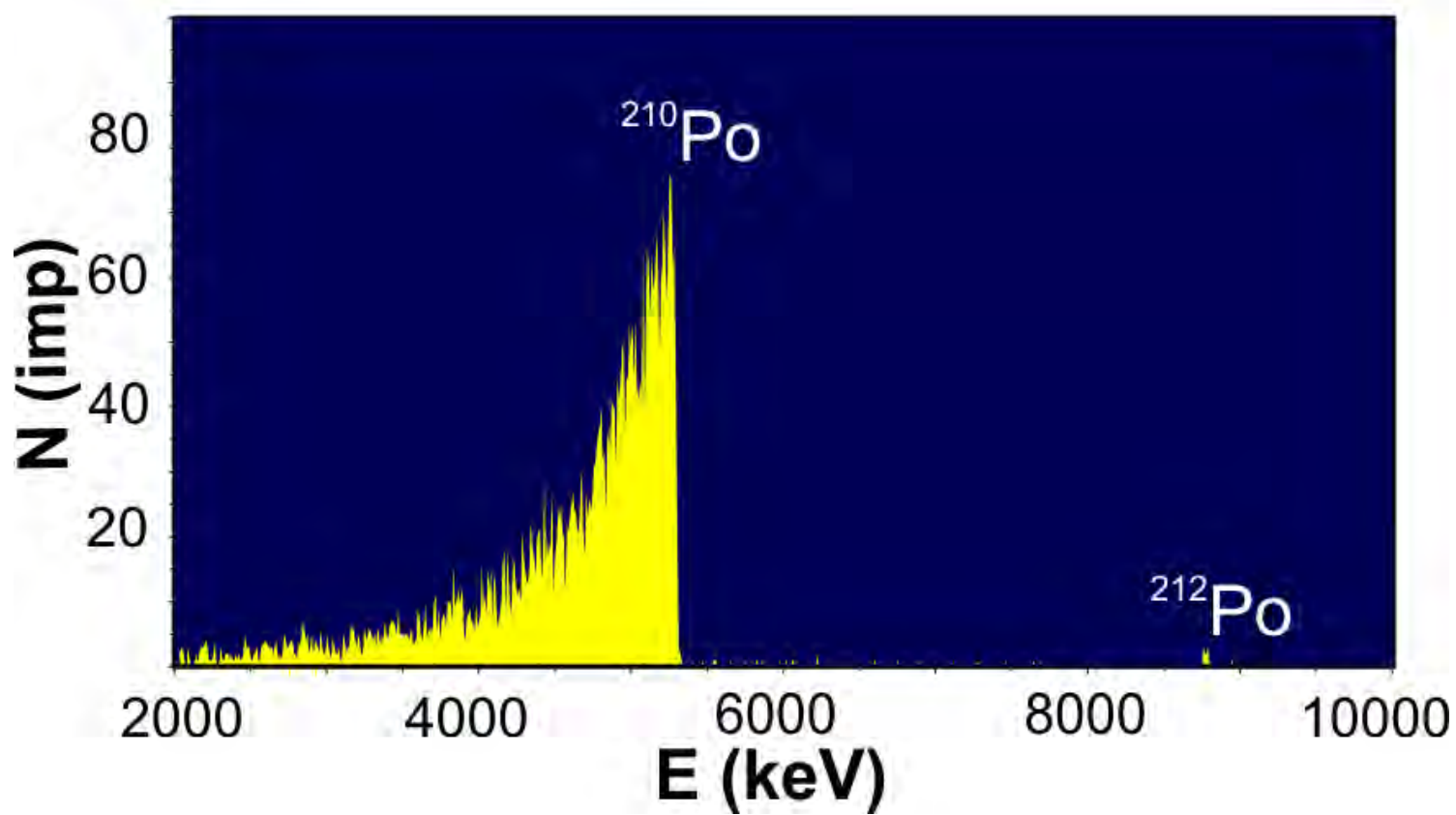


Figure 7

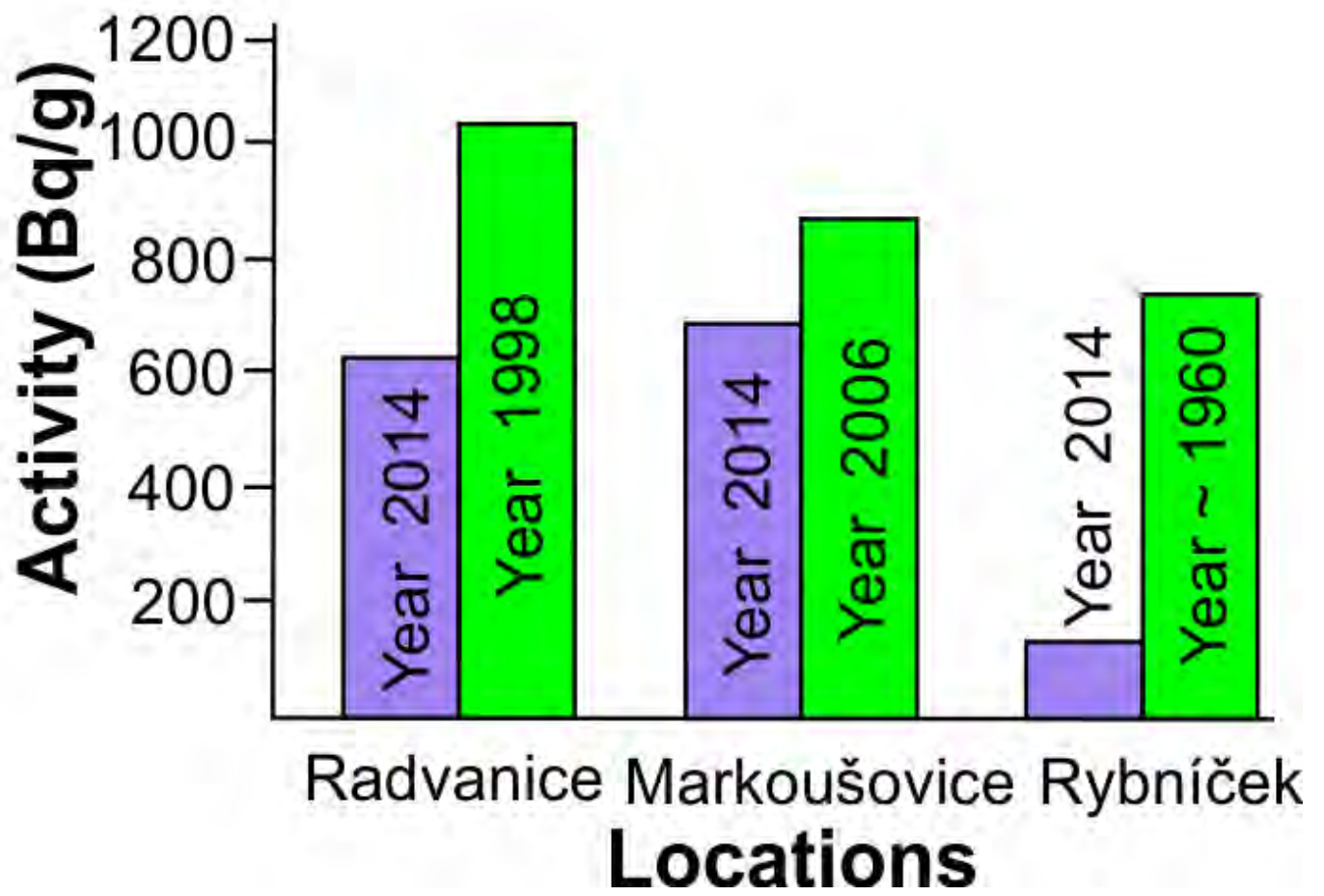


Figure 8

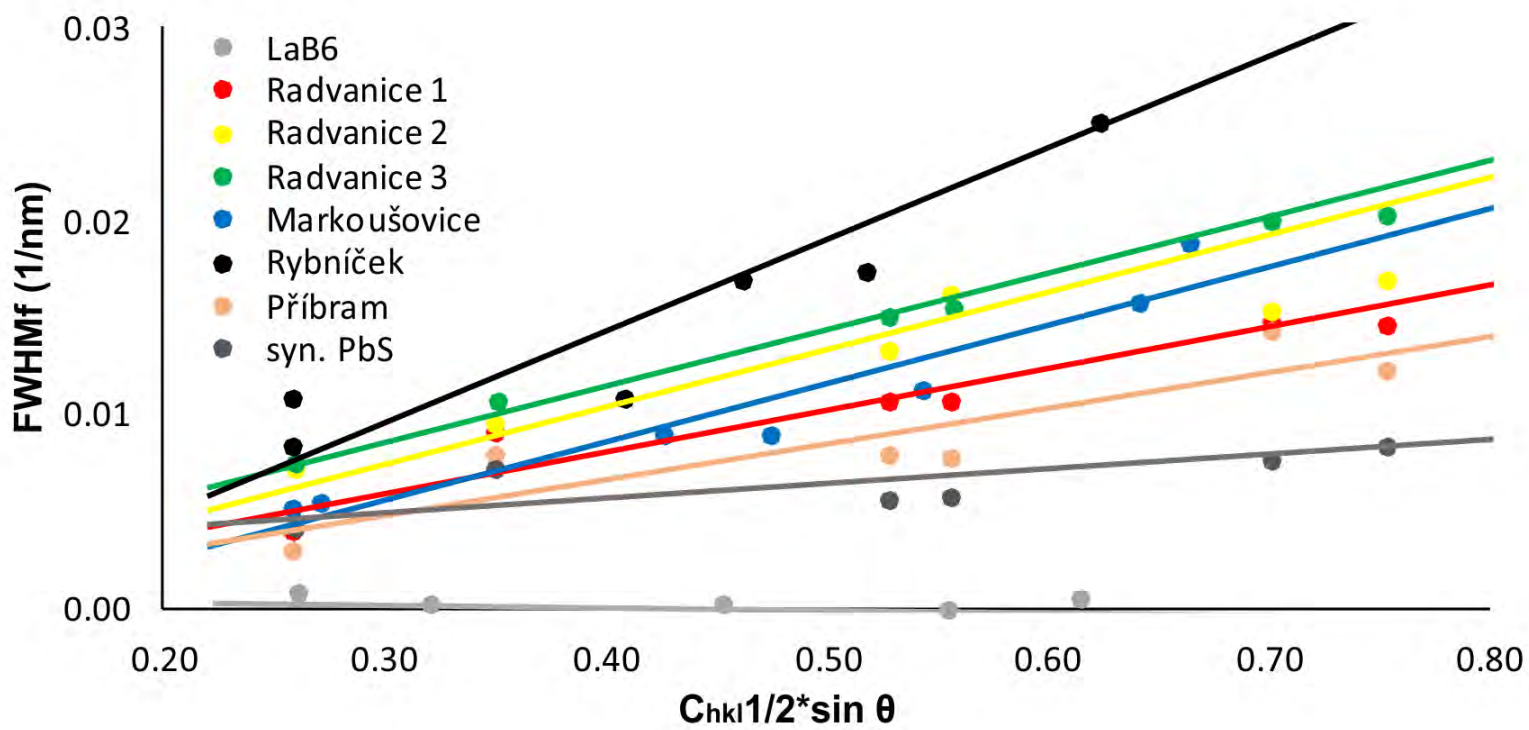


Figure 9

